View metadata, citation and similar papers at core.ac.uk

brought to you by CORE

provided by Elsevier - Publisher Connector

Available online at www.sciencedirect.com

ScienceDirect

Developmental Biology 305 (2007) 262–275

DEVELOPMENTAL BIOLOGY

www.elsevier.com/locate/ydbio

Developmental increase in the amount of rapsyn per acetylcholine receptor promotes postsynaptic receptor packing and stability

Othon L. Gervásio, Paul F. Armson, William D. Phillips *

School of Medical Sciences (Physiology), Bosch Institute, University of Sydney, Sydney, Australia

Received for publication 5 September 2006; revised 6 February 2007; accepted 9 February 2007
Available online 16 February 2007

Abstract

Neuromuscular synaptic transmission depends upon tight packing of acetylcholine receptors (AChRs) into postsynaptic AChR aggregates, but not all postsynaptic AChRs are aggregated. Here we describe a new confocal Fluorescence Resonance Energy Transfer (FRET) assay for semi-quantitative comparison of the degree to which AChRs are aggregated at synapses. During the first month of postnatal life the mouse tibialis anterior muscle showed increases both in the number of postsynaptic AChRs and the efficiency with which AChR was aggregated (by FRET). There was a concurrent two-fold increase in immunofluorescent labeling for the AChR-associated cytoplasmic protein, rapsyn. When 1-month old muscle was denervated, postsynaptic rapsyn immunostaining was reduced, as was the efficiency of AChR aggregation. *In vivo* electroporation of rapsyn-EGFP into muscle fibers increased postsynaptic rapsyn levels. Those synapses with higher ratios of rapsyn-EGFP to AChR displayed a slower metabolic turnover of AChR. Conversely, the reduction of postsynaptic rapsyn after denervation was accompanied by an acceleration of AChR turnover. Thus, a developmental increase in the amount of rapsyn targeted to the postsynaptic membrane may drive enhanced postsynaptic AChRs aggregation and AChR stability within the postsynaptic membrane.
© 2007 Elsevier Inc. All rights reserved.

Keywords: Synaptic plasticity; Synaptogenesis; Receptor trafficking; Nicotinic; Neuromuscular junction; FRET; Endplate; Receptor clustering; Acetylcholine receptor

Introduction

During embryogenesis, neural agrin, secreted from motor nerve terminals, acts as a positive regulator of the growth and stability of postsynaptic acetylcholine receptor (AChR) clusters at the primitive neuromuscular synapse (Gautam et al., 1996; Lin et al., 2005). Neural agrin activates the Muscle Specific Kinase (MuSK) and downstream signaling processes that reorganize the actin cytoskeleton, phosphorylate the AChR β-subunit and recruit AChRs into clusters (Bezakova and Ruegg, 2003; Campagna and Fallon, 2006; Glass et al., 1996; Strochlic et al., 2005; Zhu et al., 2006). Neural agrin/MuSK signaling can thus stabilize AChR clusters. The precise downstream effector mechanisms remain to be defined. They are likely to involve the cytoplasmic AChR-associated protein, rapsyn. Rapsyn is essential for forming postsynaptic AChR clusters during embryogenesis (Gautam et al., 1995) and can cluster AChRs when co-transfected into cultured heterologous cells (Froehner et al., 1990; Phillips et al., 1991). Rapsyn is thought to bind the cytoplasmic domains of the AChR, recruiting them into AChR clusters (Ramarao et al., 2001). Rapsyn mutations in humans lead to congenital Myasthenia Gravis, indicating that rapsyn continues to play a role at the synapse, well into postnatal life (Ohno et al., 2002).

Rapsyn has previously been thought to bind each AChR in a stable 1:1 ratio (Burden et al., 1983; LaRochelle and Froehner, 1987) but recent observations suggest that the stoichiometry may increase during development. When added to myotube cultures, neural agrin increased the amount of rapsyn that could be co-precipitated with each cell-surface AChR in α-bungarotoxin pull-down experiments (Moransard et al., 2003; Zhu et al., 2006). This increase in rapsyn-to-AChR stoichiometry was associated with tighter linkage of AChRs to the cytoskeleton. Furthermore, when expression plasmid for rapsyn was introduced into muscles of one-month postnatal mice the elevated postsynaptic rapsyn prolonged the retention of AChRs in the

* Corresponding author. Discipline of Physiology, Anderson Stuart Bldg. (F13), The University of Sydney, NSW 2006, Australia. Fax: +61 2 9351 2058.
E-mail address: billp@medsci.usyd.edu.au (W.D. Phillips).

0012-1606/$ - see front matter © 2007 Elsevier Inc. All rights reserved.
doi:10.1016/j.ydbio.2007.02.008

postsynaptic membrane (Gervásio and Phillips, 2005; Losen et al., 2005). Together these studies indicate that the ratio of rapsyn-to-AChR in the postsynaptic membrane is not necessarily fixed, and that increased rapsyn has the potential to stabilize postsynaptic AChRs. The relevance of this to normal development requires investigation.

The first few weeks of postnatal life in rodents are marked by activity-dependent synapse elimination (Sanes and Lichtman, 2001). During this period the postsynaptic AChR plaque becomes less plastic and more stable. At the mature synapse, postsynaptic AChRs are aggregated ($\sim$10,000 μm^{-2}) at the electron-dense 'lips' of the postjunctional membrane infoldings (Mathews-Bellinger and Salpeter, 1983). AChRs are also present deep in the membrane infoldings, but at a lower planar density. It is the aggregated AChRs that are thought to conduct the fast rise-time, high-amplitude postsynaptic current (Land et al., 1980). What factors control the proportions of aggregated and non-aggregated AChRs within the developing postsynaptic membrane? Here we describe a new Fluorescence Resonance Energy Transfer (FRET) assay that specifically detects the packing of postsynaptic AChRs into aggregates (AChRs separated by <100 Å). FRET revealed that as the synapse matured postsynaptic AChRs became more efficiently packed into aggregates. We propose that developmental changes in AChR packing and AChR turnover at the synapse might be the result of quantitative shifts in the amount of rapsyn protein within the postsynaptic membrane.

Materials and methods

Animals and surgery

Female FVB strain mice were used (Animal Resources Centre, Murdoch, WA Australia). For all denervation experiments 1-month postnatal mice were anesthetized with a mixture of ketamine and xylazine (50 mg/kg of each; Troy Laboratories, Australia) in sterile isotonic saline, as previously described (Gervásio and Phillips, 2005). The left sciatic nerve was exposed at mid-thigh. Approximately 2–3 mm of the nerve was resected in order to prevent reinnervation. The contralateral leg was used as a control. Mice were injected twice with buprenorphine (subcutaneous, 12 hourly; 0.03 mg/kg, Reckitt Benckiser, Australia). After recovery from anesthesia mice were returned to the cage for 10 days. Mice were killed by anesthesia as above followed by cervical dislocation.

Electroporation of the tibialis anterior muscle was conducted as previously described (Gervásio and Phillips, 2005). One-month postnatal mice were anesthetized as above. The lateral surface of the muscle was exposed and expression plasmid encoding rapsyn-EGFP was layered over the surface of the muscle. Silver wire electrodes were placed into the solution perpendicular to the long axis of the muscle but not touching it. Six monopolar pulses were applied (200 V/cm, duration 50 ms, 1 Hz). After removing excess solution, the wound was sutured. Mice were given a single injection of buprenorphine as described above and returned to their cage for recovery. The project was approved by the Animal Ethics Committee of the University of Sydney.

Immunofluorescence and AChR labeling

In order to measure the AChR-rich postsynaptic area, mice were anesthetized and the lateral surface of the tibialis anterior muscle was surgically exposed. Tetramethylrhodamine isothiocyanate-α-bungarotoxin (TRITC-α-BGT, 10 μg/ml; Molecular Probes, Eugene, OR) was layered over the muscle surface *in situ* for 1 h at room temperature (RT). This concentration of TRITC-α-BGT was sufficient to saturate all the AChRs at the synapse (Gervásio and Phillips, 2005). Unbound TRITC-α-BGT was removed by washing 3 times with sterile PBS. Synapses were imaged using a Nikon Eclipse E600FN upright microscope (×63 water-immersion objective, NA 1.0; Nikon, Japan) coupled to a cooled CCD camera with filter sets as previously described (Gervásio and Phillips, 2005). All the settings were kept constant during the imaging session.

For developmental analysis, the tibialis anterior muscle (for mice >1-day postnatal) or the entire shank musculature (in the case of 18-day embryonic (E18) or 1-day postnatal mice) was embedded in Tissue TEK compound (Sakura Finetek, Torrance, CA) and snap-frozen in liquid nitrogen. Transverse muscle cryosections (12 μm) were used for immunofluorescence and FRET analysis. After drying onto slides, sections were fixed with 2% paraformaldehyde in PBS for 20 min then washed with PBS. Non-specific binding was blocked by pre-incubation of sections with 1% BSA in PBS. Rapsyn was then labeled with monoclonal antibodies mab1234 or mab1579 (kind gifts from Dr S.C. Froehner; LaRochelle and Froehner, 1987). Hybridoma supernatants were diluted 1:2 in 0.1% BSA/PBS and incubated overnight at 4 °C. After washing sections 3 times in PBS, sections were further incubated with goat anti-mouse IgG conjugated to Alexa555 (Molecular Probes) for 1 h at RT. AChRs on the same sections were labeled in the same incubations using Alexa647-α-BGT (10 μg/ml; Molecular Probes). Slides were washed 3 times in PBS and mounted in 1,4-diazabicyclo {2.2.2}octane anti-fading solution (25 mg/ml in 90% glycerol/TRIS pH 8). Immunofluorescence with antiserum against syntaxin I was used to determine the effectiveness of denervation (Noakes et al., 1999). Chemicals were obtained from Sigma (St Louis) unless otherwise indicated.

To selectively label surface-exposed AChR, mice were anesthetized and the lateral surface of the tibialis anterior muscle layered over with TRITC-α-BGT (10 μg/ml for 1 h; Molecular Probes). The muscle was then washed 3 times with PBS and snap-frozen for cryosectioning. In another group of mice the muscle surface was incubated with biotin-α-BGT to saturate surface-exposed AChRs (10 μg/ml for 1 h; Molecular Probes). After washing 3 times with PBS, the muscle was dissected and frozen for cryosectioning. Transverse cryosections were fixed in 2% paraformaldehyde (20 min, RT), washed and incubated with a mixture of Alexa350-NeutrAvidin and TRITC-α-BGT (50 μg/ml and 10 μg/ml respectively, 1 h at RT; Molecular Probes). The fluorescence of Alexa350 (surface AChRs) was used to identify synapses under the microscope while the TRITC fluorescence revealed the closely associated intracellular pool of AChR. Denervated and innervated contra-lateral control muscles were compared. The slides from the four treatment groups (innervated vs. denervated AChR; surface vs. intracellular AChR) were processed, labeled and imaged together.

To test the effect of denervation upon detergent extractability of synaptic AChRs (Fig. 9), transverse cryosections were fixed for 20 min at RT with sodium *m*-periodate (21 mg/ml), L-lysine hydrochloride (180 mg/ml) and paraformaldehyde (20 mg/ml) in the presence or absence of saponin (1 mg/ml). Sections were then further extracted with 1% Triton X100 prior to washing 3× with PBS and labeling with Alexa647-α-BGT as described above. Control sections were fixed with paraformaldehyde without detergent treatment.

Confocal microscopy and FRET

For quantitation of fluorescence intensity and FRET, transverse muscle cryosections were imaged by confocal scanning laser microscopy (×63, NA 1.2 water-immersion objective; Leica DM IRE2 inverted microscope equipped with a Leica TCS SP2 system, Germany). The confocal aperture was set to 1.0 Airy unit. The Argon laser (488) was used for excitation of EGFP (15% power; emission 505–530 nm) and the He/Ne laser (543/633) was used for excitation of TRITC, Alexa555 and Alexa647 (50% power for 543 laser line, emission 560–600 nm; 25% power for 633 laser line, emission 650–710 nm). All the settings (aperture, gain and laser power) were determined at the beginning of the imaging session and were not changed.

Fluorescence Resonance Energy Transfer (FRET) was used to measure AChR aggregation at the synapse. A mixture of TRITC-α-BGT (donor fluorophor) and Alexa647-α-BGT (acceptor) was chosen for the FRET (Steigmiller et al., 2004). These were mixed and allowed to bind randomly to the AChR as described under Results. FRET is possible between two α-bungarotoxin molecules bound to the same AChR (*intra*-AChR FRET). The efficiency of *intra*-AChR FRET was estimated by transfecting expression plasmids for all four subunits of the AChR together (α, β, ε and δ) into the quail fibroblast cell line, QT6 (Phillips et al., 1997). AChRs were labeled with a mixture of TRITC-α-

BGT and Alexa647-α-BGT (2.5 μg/ml and 10 μg/ml respectively; Molecular Probes). The photobleaching of acceptor method was used to assess FRET efficiency (Eq. (a) below; Bastiaens et al., 1996; Kenworthy, 2001). FRET efficiency (E) was calculated from the increase of the fluorescence intensity of the donor (F) after the acceptor fluorophor was selectively photobleached (acceptor photobleached; AP) for all situations in which the fluorescence of donor increases after the photobleaching of the acceptor (Eq. (b)):

$$E = \frac{F^{\text{After AP}} - F^{\text{Before AP}}}{F^{\text{After AP}}} \quad \text{(a)}$$

$$F^{\text{After AP}} > F^{\text{Before AP}} \quad \text{(b)}$$

For randomly distributed donors and acceptors, FRET efficiency should increase with increasing acceptor population, as the probability of an acceptor co-localizing adjacent a potential donor increases (Wallrabe et al., 2003a). Different molar ratios of acceptor to donor were tested to achieve maximum energy transfer. The ratio of 4:1 (acceptor:donor) was chosen as it produced maximum FRET efficiency (Fig. 7C). For FRET experiments, a region of interest within each synapse (or QT6 cell) was selectively exposed to 10 scans of the 633 nm laser line at 100% power. This was sufficient to photobleach the Alexa647acceptor. The whole synapse was imaged at lower laser intensity for both donor and acceptor optical channels immediately before and after the bleaching of acceptor. In order to analyze emission spectra (Fig. 7A), synapses were labeled with TRITC-α-BGT, Alexa647-α-BGT or the mixture. Confocal optical sections of the synapse were excited with the 543 nm line and images captured at wavelengths ranging from 550 to 750 nm with increments of 4 nm.

Estimation of the absolute distance between the donor and acceptor fluorophor is problematic. The theoretical relationships between FRET efficiency and donor–acceptor distance are described in Eqs. (c) (d) (e) below (Van Der Meer et al., 1994):

$$E = R_o^6/(R_o^6 + R^6) \quad \text{(c)}$$

and

$$R_o^6 = (8.79 \times 10^{23})\kappa^2 n^{-4} \Phi_d J \text{Å}^6 \quad \text{(d)}$$

where E is the efficiency of resonance energy transfer, R_o is the donor–acceptor distance at which transfer efficiency is 50%, R is the distance separating the donor and acceptor, Φ_d is the quantum efficiency of the donor, κ^2 is the orientation factor; n is the refractive index of the solvent and J is the overlap integral between the donor fluorescence and the acceptor absorption, defined as

$$J = \int f_D(\lambda)\varepsilon_A(\lambda)\lambda^4 d\lambda \quad \text{(e)}$$

where λ is the wavelength, $\varepsilon_A(\lambda)$ is the molar extinction coefficient of the acceptor at that wavelength and f_D is the fluorescence spectrum of the donor normalized on the wavelength scale (Van Der Meer et al., 1994). Published values for these factors can differ substantially for a given dye depending upon the solvent and the specific protein to which the fluorophor was attached (Panchuk-Voloshina et al., 1999; Soper et al., 1993).

Measurement of AChR turnover

Muscles were denervated at 1-month postnatal (as described above) and AChR turnover was assessed 10 days after sciatic nerve section. Mice were anesthetized and the lateral surface of the tibialis anterior muscle was surgically exposed on both legs (denervated and innervated control). AChRs exposed on the surface of the muscle were labeled by incubation with FITC-α-BGT (10 μg/ml, Molecular Probes) for 1 h. Half of the mice were killed and the muscles snap frozen immediately after labeling (Day 0 controls). The remaining mice were allowed to recover and were monitored for a further 10 days (Day 10—after labeling). Transverse cryosections were fixed, washed with PBS and labeled with Alexa647-α-BGT (10 μg/ml). Controls and experimental samples were sectioned, labeled and imaged together. The FITC fluorescence revealed the level of original AChRs remaining at the synapse 0 or 10 days after the initial labeling. The Alexa647 fluorescence provided a comparative measure of the level of newly added AChR (Fig. 6).

Image and statistical analysis

ImageTool 3.00 software (The University of Texas Health Science Center, San Antonio TX; http://ddsdx.uthscsa.edu/dig/itdesc.html) was used for quantitation of fluorescence intensity and area. The background fluorescence of regions surrounding the synapse was subtracted from the regions of interest. To measure the AChR-rich area (see Figs. 3I–K), a Z-stack of the synapse was performed *in vivo* (increments of 1 μm) using the fluorescence microscope after labeling the AChRs with TRITC-α-BGT. A Z-projection was then performed using ImageJ 1.31v software (NIH, Bethesda; http://rsb.info.nih.gov/ij/). An arbitrary threshold was applied to all images to create the binary image (black pixels in Fig. 3J). Pixel counting was used to determine the AChR-rich area in μm^2 (Fig. 3K). The relationships between two independent variables (rapsyn-EGFP and AChR in Figs. 1C and D; FRET efficiency and acceptor/donor ratio in Fig. 7B; FRET efficiency and AChR level in Fig. 8B) were determined by Pearson's correlation (R^2 coefficient of determination). Student's t-test (two-tailed) was used to compare means of two different groups. Analysis of variance (ANOVA) was used in situations of more than 2 groups (one-way ANOVA: 7C and 8E) or more than 2 variables (two-way ANOVA: Figs. 1E, 4, 6 and 8D)). Mean and standard error of the mean (SEM) are shown for each group.

Results

The stability of postsynaptic AChR varies with the amount of rapsyn

When rapsyn-EGFP was electroporated into fibers of the tibialis anterior muscle of 1-month old mice, it became closely co-localized with postsynaptic AChR (Figs. 1A, B). AChRs were labeled with TRITC-α-bungarotoxin (TRITC-α-BGT), a toxin that binds to AChRs in an effectively irreversible manner (Akaaboune et al., 2002; Berg and Hall, 1975). The intensity of rapsyn-EGFP fluorescence (Rapsyn-EGFP level) varied considerably from synapse to synapse, presumably reflecting differing uptake of the rapsyn-EGFP expression plasmid among electroporated fibers. The intensity of AChR labeling (AChR level) also varied somewhat from synapse to synapse. However, for mice killed immediately after TRITC-α-BGT labeling there was no correlation between AChR level and rapsyn-EGFP level (Fig. 1C). This confirms that increased rapsyn had no effect upon the steady-state level of postsynaptic AChRs (Gervásio and Phillips, 2005). In contrast, when muscles were fixed and analyzed 4-days after pulse-labeling AChRs, the intensity of residual α-bungarotoxin-labeling at individual synapses (AChR level) was positively correlated with the intensity of their rapsyn-EGFP fluorescence (rapsyn-EGFP level; Fig. 1D). Synapses with the highest level of rapsyn-EGFP retained significantly more α-bungarotoxin-labeled AChR over the 4-days than those with low levels of rapsyn-EGFP or those with no rapsyn-EGFP at all (Fig. 1E).

In follow-up experiments, mice left for differing numbers of days after labeling were processed and imaged together in the same confocal session, making possible quantitative comparison of postsynaptic fluorescence intensities. Postsynaptic AChRs were pulse-labeled with TRITC-α-BGT as above and mice were killed either 0, 6 or 10 days later. Scatter plots of the type shown

in Figs. 1C and D were constructed and least-squares lines-of-best-fit were calculated. For synapses imaged 6 and 10 days after pulse-labeling, the intensity of residual labeled AChR level was correlated with rapsyn-EGFP-level at the same synapse. For each scatter plot the correlation was highly significant ($P<0.001$ by Pearson's correlation; scatter plots not shown). The slope of the correlation increased with time after AChR pulse labeling, demonstrating that the retention of labeled postsynaptic AChR was dependent both on time, and on the amount of rapsyn-EGFP in the postsynaptic membrane (Fig. 1F).

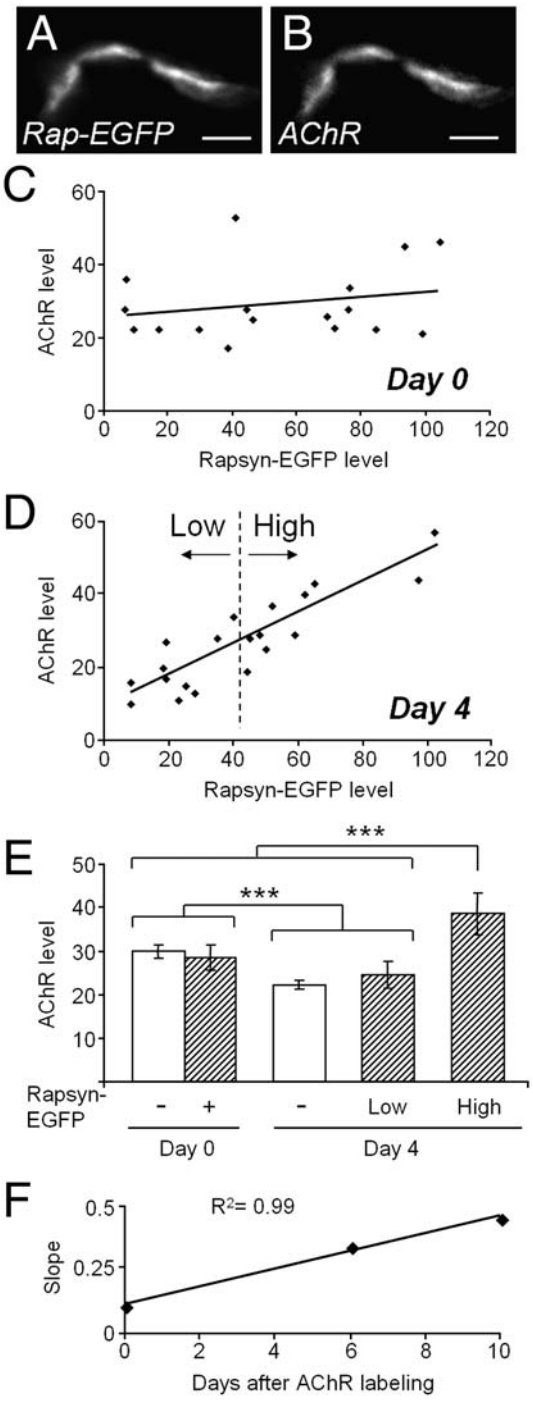

Fig. 1. Retention of AChR within the postsynaptic membrane varies with the density of postsynaptic rapsyn-EGFP. Tibialis anterior muscles of 1-month old mice were electroporated with rapsyn-EGFP. Seven days later AChRs on the surface of the muscle were labeled with TRITC-α-BGT. (A and B) A confocal transverse section of a synapse reveals co-localized rapsyn-EGFP (Rap-EGFP) and TRITC-α-BGT labeling (AChR). (C and D) Mean pixel intensity values for TRITC-α-BGT (AChR level) were plotted against those of rapsyn-EGFP (Rapsyn-EGFP level) for individual synapses. For muscles imaged immediately after TRITC-α-BGT labeling (Day 0) there was no relationship between rapsyn-EGFP level and AChR level (C; $R^2=0.051$; $P>0.05$; Pearson's correlation). For synapses imaged 4 days after TRITC-α-BGT pulse-labeling (Day 4) a direct relationship emerged (D; $R^2=0.82$; $P<0.001$). (E) Arbitrary division of synapses into those displaying low and high rapsyn-EGFP (vertical dotted line in panel D) confirmed that synapses with high levels of rapsyn-EGFP retained more AChR over the 4-day period than those with low levels of rapsyn-EGFP or no rapsyn-EGFP at all (***$P<0.001$, ANOVA). (F) An experiment in which muscles were processed and analyzed together 0, 6 or 10 days after pulse-labeling with TRITC-α-BGT so as to permit quantitative comparison of slopes. At each time point the correlation was highly significant ($P<0.001$ by Pearson's correlation, individual scatter plots not shown). The slope for the lines-of-best-fit increased with time after TRITC-α-BGT pulse-labeling (Days 0, 6 and 10). Thus, the synapses with the most rapsyn-EGFP retained the most TRITC-α-BGT-labeled AChR for the greatest time. Data in panels C and D each represent individual synapses from 3 mice imaged in the same session. Bars in E represent mean±SEM for 3 mice in each group with a minimum of 7 synapses per mouse. Scale bar in A and B=5 μm.

Developmental changes in postsynaptic rapsyn-to-AChR ratio

Confocal immunofluorescence imaging revealed changes in the level of endogenous AChR and rapsyn at the synapse during postnatal synaptic maturation. The intensity with which the postsynaptic membrane stained for AChR with fluorescent-α-BGT (AChR level) increased from embryonic Day 18 to reach a plateau value at about 1-month postnatal (Fig. 2A). The intensity of anti-rapsyn immunofluorescence increased over a similar time-course, but to an even greater degree than for AChR (not shown). Hence the ratio of postsynaptic anti-rapsyn immunofluorescence relative to α-BGT fluorescence (hereafter referred to as the rapsyn-to-AChR immunofluorescence ratio) rose about two-fold, reaching a plateau value by one-month postnatal (Fig. 2B).

We examined the effects of denervation at 1-month postnatal. Ten days after sciatic nerve section, the presynaptic marker, syntaxin I had disappeared from over the postsynaptic AChRs, confirming denervation (Figs. 3A–D). Muscle fibers showed substantial atrophy, compared to innervated, contralateral fibers. Muscle weight and muscle fiber cross-sectional area were both reduced (Figs. 3E–H). Analysis of *en face* images showed that the area occupied by the AChR-rich 'postsynaptic' membrane did not change after denervation (Figs. 3I–K). However, the AChR level (intensity of fluorescent-α-BGT labeling) was increased, both within the AChR-rich area and in the adjacent 'perisynaptic' membrane areas (Figs. 4A, B). We repeated these experiments, separately labeling surface-exposed AChRs on live, intact muscle fibers and intracellular AChRs (exposed by cryosectioning). This showed that within the AChR-rich area about 90% of the AChRs were exposed on the cell surface, both before and after denervation (Fig. 4C). Thus, denervation caused no detectable change in the area rich in AChRs, but significantly increased the number of surface-exposed AChRs within the

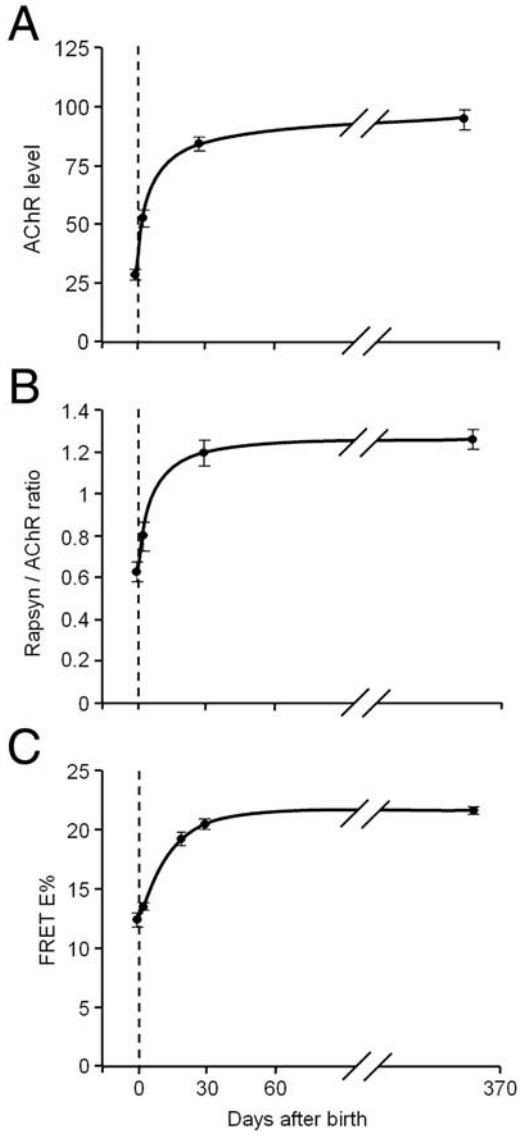

Fig. 2. Developmental increase in postsynaptic AChR packing and in the rapsyn-to-AChR immunofluorescence ratio in the tibialis anterior muscle. Between embryonic Day 18 and 1 month postnatal there were increases in the: (A) intensity of Alexa647-α-BGT staining of the postsynaptic membrane, reflecting the average density of AChRs (AChR level), (B) ratio of the intensities of anti-rapsyn immunofluorescence and Alexa647-α-BGT fluorescence (rapsyn-to-AChR immunofluorescence ratio) and (C) the efficiency of Fluorescence Resonance Energy Transfer between postsynaptic α-bungarotoxin binding sites (FRET E%). FRET provided a gauge of the degree to which AChRs were aggregated in the postsynaptic membrane (see Results). Data represent the mean±SEM for 3 mice at each age with a minimum of 8 synapses per mouse.

AChR-rich area. These results are consistent with electron microscopic autoradiographic studies on the sternomastoid muscle showing a ~1.3-fold increase in postsynaptic AChR density 7 days after nerve crush (Szabo et al., 2003).

While the number of postsynaptic AChRs rose after denervation, on average there was less rapsyn associated with each AChR. Two monoclonal anti-rapsyn antibodies that recognize distinct parts of the rapsyn protein (Gervásio and Phillips, 2005; LaRochelle and Froehner, 1987) revealed a reduction (~24–46%) in the rapsyn-to-AChR immunofluorescence ratio after denervation (Fig. 5). To verify this drop we electroporated rapsyn-EGFP into muscle fibers prior to denervation. Twelve days after denervation the intensity of 'postsynaptic' rapsyn-EGFP fluorescence was 53% lower for denervated synapses compared to contralateral innervated synapses ($P<0.001$; $n=10$ synapses, Student's t-test; data not shown). Together these results suggest that denervation reduces the amount of rapsyn targeted to the postsynaptic membrane (rapsyn levels reverting toward those characteristic of neonatal synapses).

Accelerated postsynaptic AChR turnover following denervation

AChR turnover was assessed by pulse-labeling AChRs at synapses on the lateral surface of the tibialis anterior muscle with fluorescent-α-BGT, at 1-month postnatal. Mice were killed and muscles-frozen immediately after labeling (Day 0; Figs. 6A, B) or 10-days later (Figs. 6C, D). Cryosections of all treatment groups were processed and imaged together to permit quantitative comparison (see Materials and methods). For innervated muscles, about half of the labeled AChRs were retained within the AChR-rich area 10 days after labeling (Fig. 6G, compare open bars for Day 0 and Day 10). This is consistent with the commonly reported half-life of ~10 days for AChRs in adult muscles (Akaaboune et al., 1999; Bezakova et al., 2001b; Salpeter and Harris, 1983). Once again denervation significantly increased the AChR level in the AChR-rich area (Fig. 6G, compare open and filled bars for Day 0). However, with denervated synapses a greater fraction of the α-BGT-labeled AChRs present at 0 days were subsequently lost by 10 days (Fig. 6G, compare filled bars for Day 0 and Day 10). The delivery of newly synthesized AChRs to the AChR-rich area was accelerated after denervation, compensating for the greater rate of AChR loss (Fig. 6H). Thus, the reduction in the rapsyn-to-AChR immunofluorescence ratio after denervation was associated with an accelerated turnover (loss and replacement) of AChRs within the AChR-rich area.

Fluorescence Resonance Energy Transfer (FRET) provides a new measure of AChR clustering

At the ultrastructural level the mature postsynaptic membrane is divided into a repeating pattern of AChR-aggregate-containing domains and deep membrane infoldings in which AChRs are present at one-tenth the planar density (Salpeter and Harris, 1983). The location of the AChR aggregates immediately beneath sites of presynaptic transmitter release underpins the fast rise-time, high-amplitude postsynaptic current (Land et al., 1980). Our confocal images of fluorescent-α-BGT labeling did not resolve AChR aggregate domains from folds. Thus, the fluorescence intensity measurements (AChR level) represent a spatial average of AChR density across the highly folded postsynaptic membrane.

A confocal Fluorescence Resonance Energy Transfer (FRET; Sekar and Periasamy, 2003) method was developed to measure the degree to which postsynaptic AChRs were packed into aggregates in the AChR-rich postsynaptic membrane. For the

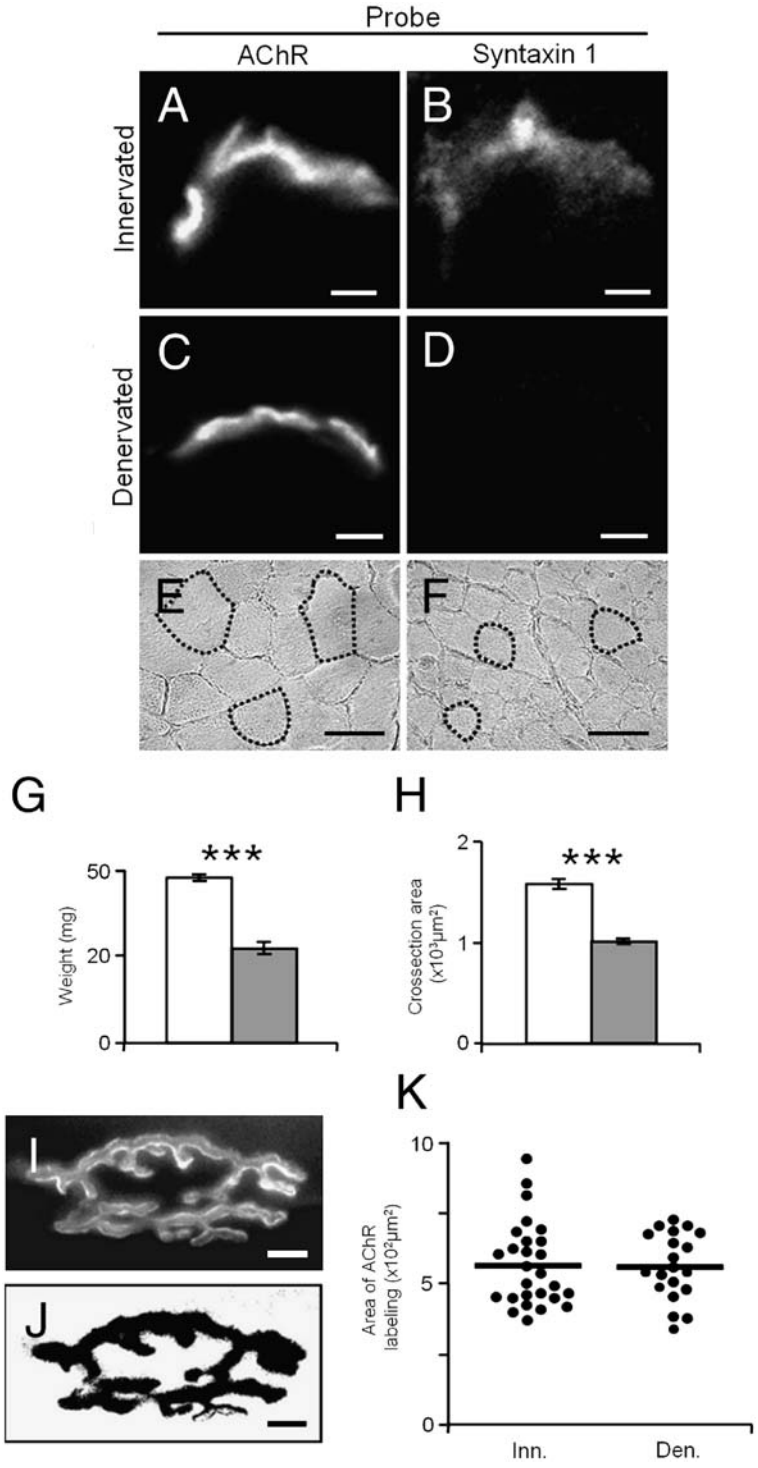

Fig. 3. Changes in the tibialis anterior muscle following denervation in one-month old mice. (A and C) Ten days after sciatic nerve section synaptic AChR clusters were still present at denervated synapses (transverse sections showing Alexa647-α-BGT staining). (B and D) The overlying immunostaining for the presynaptic membrane protein, syntaxin I, had disappeared. Transmitted light images revealed muscle fiber atrophy in denervated muscle (F) compared to innervated muscle (E). Dotted lines in panels E and F mark the circumference of sample muscle fibers. Denervated muscles (filled bars) showed reduced muscle weight (G) and cross-sectional area (H) compared to innervated muscles (open bars). (I) Synapses labeled with Alexa647-α-BGT were imaged *en face.* (J) The AChR-rich area of the synapse was determined from the binary image. (K) The area rich in AChRs was not significantly different for denervated (Den.) compared to innervated (Inn.) synapses (bars show means for 3 mice, dots represent individual synapses). Bars in panels G and H show means and ± SEM for: $n = 5$ muscles in panel G and $n = 4$ mice (≥ 25 muscle fibers per mouse) in panel H (***$P < 0.001$; Student's *t*-test). Scale bars in panels A–D = 5 μm; E and F = 50 μm; I and J = 10 μm.

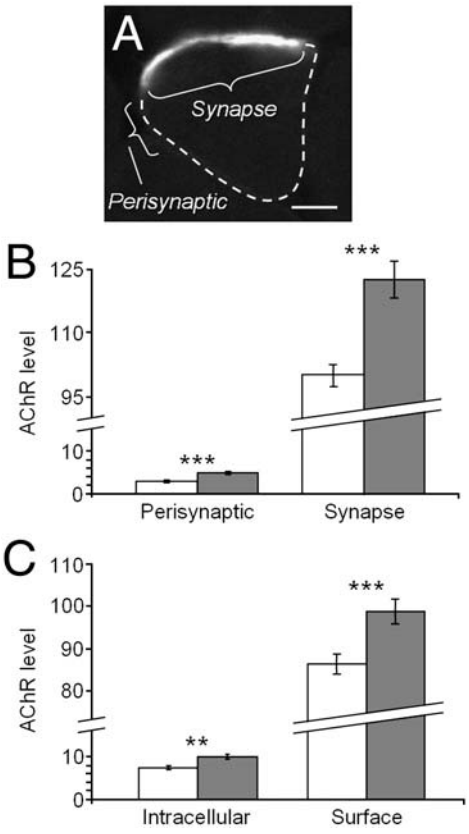

Fig. 4. Increases in postsynaptic AChR level 10 days after sciatic nerve section of 1-month old mice. (A) Transverse optical section through the AChR-rich region of a denervated tibialis anterior synapse labeled with Alexa647-α-BGT. Arrows mark the boundaries of the AChR-rich region. Dashed line outlines the perimeter of the muscle fiber (dimly labeled by Alexa647-α-BGT). A line was drawn to follow the AChR-rich 'postsynaptic' and adjacent 'perisynaptic' membrane regions as indicated. (B) Mean intensity of AChR labeling in perisynaptic and synaptic membrane regions (AChR level). Open bars represent innervated muscle fibers while filled bars denote denervated fibers. (C) AChR level for surface-exposed and intracellular AChR at innervated (open bars) and denervated (filled bars) synapses. Within the AChR-rich postsynaptic region most of the AChRs (~90%; note the break in scale) were exposed to the extracellular fluid (surface). There were significant increases in both surface and intracellular AChRs following denervation. Bars represent mean±SEM for 4 mice with minimum of 10 synapses per mouse (**$P<0.01$; ***$P<0.001$; ANOVA). Scale bar in panel A=5 μm.

FRET donor and acceptor pair, we chose α-BGT labeled with tetramethylrhodamine isothiocyanate (TRITC-) and Alexa647-, respectively (see Materials and methods). These two fluorophors were allowed to bind to postsynaptic AChRs either singly or as a mixture to test for FRET between α-BGT binding sites on AChRs. An underlying assumption of our assay is that the fluorescent toxins will bind in a random, competitive manner to the many binding sites within the postsynaptic membrane. A confocal optical section of the synapse was illuminated by the 543 nm laser line and the spectrum of emitted light was recorded. As expected, when AChRs were labeled with TRITC-α-BGT alone, red light was emitted at around 580 nm (Fig. 7A, solid line). Alexa647-α-BGT was not excited by the 543 nm line (dashed line). In contrast, when synapses were labeled with a mixture of TRITC-α-BGT and Alexa647-α-BGT, the TRITC-α-BGT emission peak at 580 nm was reduced and a second peak appeared at ~670 nm (far-red, Fig. 7A, dotted line and arrow), demonstrating resonant energy transfer from TRITC-α-BGT to Alexa647-α-BGT.

We optimized FRET efficiency. According to the donor geometric exclusion model, FRET efficiency can be maximized if each individual donor fluorophor is surrounded by several acceptor molecules (Wallrabe et al., 2003a,b). Thus, we labeled AChRs with mixtures of Alexa647-α-BGT (acceptor) and TRITC-α-BGT (donor) in various molar ratios. This yielded the expected positive correlation between the measured post-synaptic acceptor-to-donor fluorescence ratio and the FRET efficiency (Fig. 7B). A 4:1 molar concentration ratio of Alexa647-α-BGT to TRITC-α-BGT produced the highest mean FRET efficiency and was chosen for all subsequent experiments (Fig. 7C).

Efficient FRET occurred when AChRs were packed tightly together in AChR aggregates. The extracellular portion of the pentameric AChR has a diameter of about 80 Å. There are two binding sites for α-BGT, located equatorially, at the α/ε and α/δ subunit interfaces on opposite sides of the AChR (Mitra et al., 1989; Paas et al., 2003). When bound to the AChR the greater part of the toxin protein surface protrudes axially beyond the perimeter of the AChR (Samson et al., 2002). Approximately one fluorophor is bound randomly to a primary amine group on each toxin molecule. Thus, we estimate that when donor and

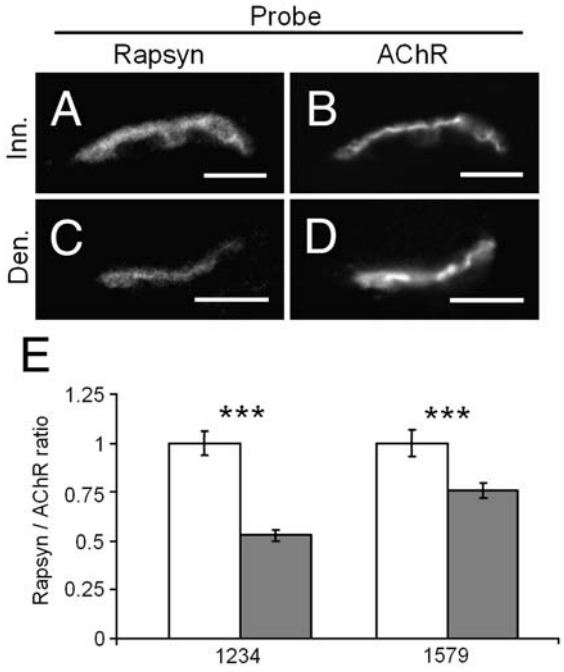

Fig. 5. Denervation reduced the rapsyn-to-AChR immunofluorescence ratio at endplates in the tibialis anterior muscle. (A–D) Transverse confocal sections of innervated (Inn.) and denervated (Den.) synapses were double labeled by immunofluorescence with anti-rapsyn antibody mab1234 and Alexa647-α-BGT to reveal AChR. (E) Denervation caused significant reductions in the rapsyn-to-AChR immunofluorescence ratio, whether this was determined using mab1234 or another anti-rapsyn antibody, mab1579 (LaRochelle and Froehner, 1987). The rapsyn-to-AChR ratio for denervated synapses (filled bars) was normalized to innervated controls (open bars) to facilitate comparison. Bars in panel E represent the mean±SEM for 4 mice with minimum of 10 synapses per mouse (***$P<0.001$; Student's t-test). Scale bar in panels A–D=10 μm.

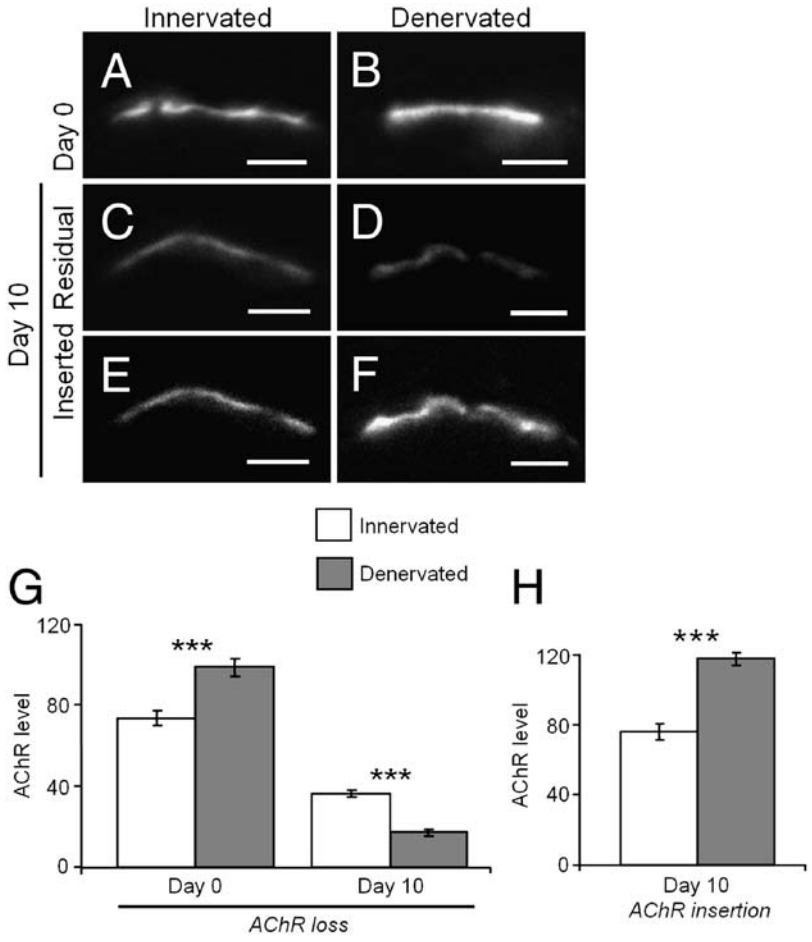

Fig. 6. Turnover of AChR accelerated after denervation in 1-month old mice. (A–F) Synapses on the lateral surface of the tibialis anterior muscle were labeled with FITC-α-BGT 10 days after sciatic nerve section. Mice were killed and transverse muscle cryosections were analyzed by confocal microscopy immediately (Day 0) or 10 days after FITC-α-BGT pulse-labeling (Day 10 residual). Newly inserted AChRs were labeled by exposing the same synapses to Alexa647-α-BGT on Day 10 (Day 10 inserted). (G) When killed immediately after FITC-α-BGT labeling, the AChR level was significantly higher for denervated synapses (Day 0, filled bar) than for innervated controls (Day 0, open bar). By Day 10 there were fewer residual FITC-α-BGT-labeled AChRs at denervated synapses than at innervated synapses. Note that since AChRs were labeled 10-day after denervation, the rate of loss of AChRs represents an average turnover for pre-existing and newly inserted postsynaptic AChRs. (H) Denervated synapses displayed more newly inserted (replacement) AChRs at Day 10. Bars in panels G and H represent mean ± SEM for 4 mice with minimum of 10 synapses per mouse (***$P<0.001$; ANOVA). Scale bar in panels A–F = 5 μm.

acceptor are bound to the same AChR they would be separated on average by about 90 Å, permitting a relatively weak, *intra-receptor FRET*. In contrast, given the high packing density of AChRs at the adult synapse (~10,000 μm^2; Salpeter and Harris, 1983), the labeled-α-BGT molecules protruding from the perimeters of adjacent AChRs should bring their attached donors and acceptors closer than 90 Å, yielding *inter-receptor FRET*, with a greater efficiency (Fig. 8A).

Experimental results bore out these predictions. FRET was measured by the increase in the intensity of donor (TRITC-α-BGT) fluorescent emission that occurred after the acceptor (Alexa647-α-BGT) was selectively photobleached (Fig. 8C). The 1-month postnatal synapse displayed high efficiencies of FRET (~24%; Fig. 8E). In contrast, when donor and acceptor fluorophors were simply spread on a glass surface in the absence of AChR, no FRET was detected (see "Solution" in Figs. 8C and D). Thus, FRET depended upon donor and acceptor binding to AChRs. FRET could be detected in situations where AChRs were not clustered, but in such cases the efficiency was low, as predicted. For example, AChRs (α, β, ε and δ subunit combination) expressed in the fibroblast cell line, QT-6, yielded a FRET efficiency of only 5% compared to 24% for AChRs at the mature synapse. For intracellular AChRs beneath the postsynaptic membrane the FRET efficiency was also low (Fig. 8D).

FRET efficiency was not correlated with TRITC-α-BGT labeling intensity (AChR level). FRET efficiency was sampled by photobleaching the acceptor within small portions of synapses of 1-month old mice (see example in Fig. 8C, lower panels). For each such sampled area the FRET efficiency was plotted against AChR level in the same area (Fig. 8B). There was considerable variability in the AChR level within and among the AChR-rich areas of 1-month old synapses. In contrast, FRET efficiency was relatively constant (Fig. 8B). There was no correlation between the AChR level (within the sampled area) and the FRET efficiency within the same area. The intensity of fluorescent labeling for receptor (AChR level) was likely influenced by factors such as submicroscopic membrane

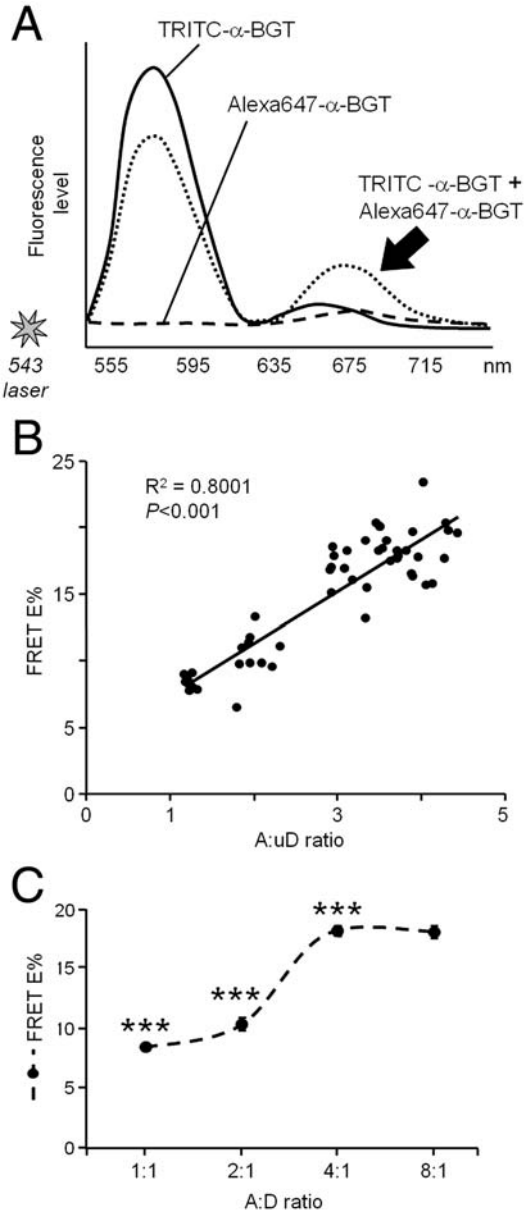

Fig. 7. Fluorescence Resonance Energy Transfer occurs between α-bungarotoxin binding sites on postsynaptic AChRs. Transverse cryosections of synapses from 1-month old mice were labeled with a mixture of TRITC-α-BGT and Alexa647-α-BGT and were analyzed by confocal microscopy. (A) Emission spectra for synaptic AChRs labeled with either TRITC-α-BGT or Alexa647-α-BGT and excited with the 543 nm laser line (solid line and dashed line respectively). TRITC-α-BGT emitted light at ~580 nm but Alexa647-α-BGT was not excited. When synapses were labeled with a mixture of the two probes (dotted line), excitation of TRITC-α-BGT at 543 nm resulted in a second emission peak at ~670 nm (black arrow), indicating resonance energy transfer between TRITC-α-BGT and Alexa647-α-BGT. (B) Individual synapses were labeled with solutions containing mixtures of TRITC-α-BGT and Alexa647-α-BGT in different proportions. For each endplate the Alexa647 fluorescence intensity was compared to TRITC fluorescence intensity (measured after photobleaching the acceptor fluorophor) to determine the proportion of α-bungarotoxin binding sites occupied by acceptor and unquenched donor (A:uD ratio). FRET efficiency (FRET E%, see Materials and methods) was positively correlated with the A:uD ratio. Dots represent individual synapses (minimum of 10 synapses per mouse; $n=4$ mice; $R^2=0.80$; $P<0.001$; Pearson's correlation). (C) FRET E% depended upon the molar ratio of Alexa647-α-BGT and TRITC-α-BGT used to label the postsynaptic AChRs (donor; A:D ratio; minimum of 10 synapses analyzed for each A:D ratio; ***$P<0.001$; ANOVA).

folding. FRET may provide a more reliable measure of the degree to which postsynaptic AChRs were aggregated.

FRET tracked with developmental increase in rapsyn-to-AChR ratio

During the first month postnatal the FRET efficiency rose roughly in parallel with the increases in AChR level and the rapsyn-to-AChR immunofluorescence ratio (Fig. 2C; the rise in AChR level representing an increase in the number of postsynaptic AChRs). We also used α-bungarotoxin conjugated to Alexa488 (donor) and Alexa647 (acceptor) as a second FRET pair. While the FRET efficiencies with Alexa488/Alexa647 differed from those obtained with TRITC/Alexa647 (reflecting fluorophor properties), we again recorded a significant increase in FRET efficiency between newborn and one-month postnatal endplates (Fig. 8E compare *newborn* vs. *synapse*; $P<0.001$, ANOVA). Within the perisynaptic region of 1-month old muscle fibers (Fig. 4A) the efficiency of FRET was significantly lower than for the adjacent synaptic region ($P<0.001$), but was not significantly different to that found within neonatal endplates (Fig. 8E).

When the muscles of one-month old mice were denervated there was a small, but highly significant (13%) reduction in FRET efficiency for surface-exposed postsynaptic AChRs (Fig. 8D, compare last two bars). The reduction in FRET efficiency could conceivably reflect either an increase in the spacing of adjacent AChRs within the AChR aggregate or a reduction in the fraction of postsynaptic AChRs that were engaged within AChR aggregates. The 13% reduction in FRET efficiency following denervation was matched by a similar decrease in the proportion of synaptic AChRs that were resistant to detergent extraction (Fig. 9, compare A and B). Resistance to detergent extraction is one measure of AChR clustering and immobilization (Moransard et al., 2003; Phillips et al., 1993). Thus, the decline in FRET efficiency following denervation may be quantitatively explained by the reduction in the fraction of detergent resistant (clustered) AChRs in the postsynaptic membrane.

Discussion

Postsynaptic AChR aggregates, arrayed precisely beneath each site of presynaptic transmitter release, are thought to mediate fast synaptic transmission at the neuromuscular synapse (Land et al., 1980; Sanes and Lichtman, 2001). The confocal FRET assay described here reveals a hitherto unknown developmental increase in the efficiency with which postsynaptic AChRs are recruited into AChR aggregates. This tightening of AChR aggregation was coincident with the transition of the plastic neonatal synaptic site into a stable, mature synapse with postjunctional membrane infoldings. The increase in AChR aggregation as measured by FRET was complete by 1-month postnatal. Denervation at this age led to a significant reduction in AChR aggregation (measured by FRET) and an acceleration of the metabolic turnover of the AChR. Parallel changes in the amount of rapsyn associated with each postsynaptic AChR suggest a mechanism that may help control the efficiency with

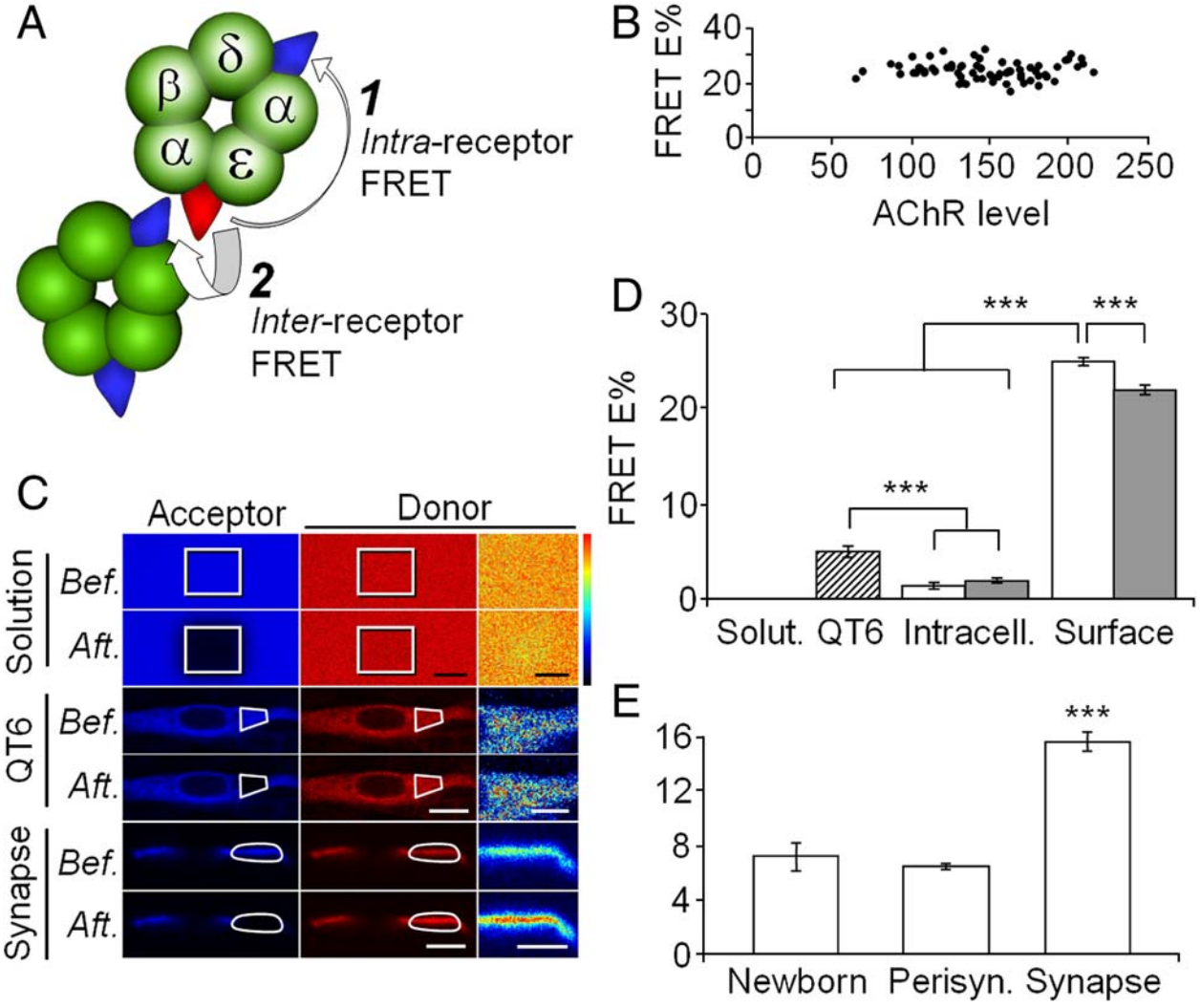

Fig. 8. FRET efficiency for postsynaptic AChRs was reduced following denervation. (A) Each AChR possesses two α-bungarotoxin binding sites so FRET is possible between the two sites within a single AChR (intra-AChR FRET; long thin arrow), but efficient FRET requires that AChRs be packed tightly together in an AChR aggregate (inter-AChR FRET, short thick arrow). Each AChR within an AChR aggregate is surrounded by several other AChRs (not shown). Given the known packing density (~10,000 μm^2), adjacent AChRs must be closely spaced, as indicated for the pair of AChRs in the cartoon. (B) Areas sampled from multiple 1-month old synapses varied considerably in their AChR level (intensity of unquenched TRITC-α-BGT fluorescence; measured after acceptor photobleach), but FRET efficiency was independent of AChR level ($n=70$ synapses; $R^2=0.0009$; $P>0.05$; Pearson's correlation). (C) Fluorescent images of TRITC-α-BGT emissions before (Bef.) and after (Aft.) selectively photobleaching the FRET acceptor (Alexa647-α-BGT) within the boxed area. Synapses of 1-month old mice revealed FRET as an increase in TRITC-α-BGT (donor) fluorescence intensity within the boxed area (C, lower panels). Spectrum/intensity scale at right applies to the right hand column of pseudocolor inset panels. FRET was low for AChRs expressed in QT-6 fibroblasts and undetectable when the mixture TRITC-α-BGT and Alexa647-α-BGT was allowed to bind to glass in the absence of AChR (Solution). (D) Comparison of the efficiency of FRET for surface and intracellular (Intracell.) AChRs at innervated synapses (open bars) and denervated synapses (filled bars) of 1-month postnatal mice. Only low efficiency FRET was detected when TRITC-α-BGT and Alexa647-α-BGT were allowed to bind to subsynaptic intracellular AChRs (Intracell.) or to AChRs expressed in QT-6 fibroblasts (QT-6). FRET could not be detected when the donor and acceptor mix was allowed to bind to glass (Solut.). (E) Efficiency of FRET in the synaptic and perisynaptic membranes of 1-month old muscles and at synapses in newborn mice using Alexa488-α-BGT and Alexa647-α-BGT as an alternative donor/acceptor pair. Error bars represent mean ± SEM for $n=30$ cells (QT-6), $n=4$ mice (Intracell., Surface and Synapse), $n=5$ mice (Newborn) and $n=3$ mice (Perisyn.). FRET was measured at a minimum of 15 endplates for each mouse (***$P<0.001$; ANOVA). Scale bars = 10 μm for Solution and QT-6, 5 μm for Synapse).

which AChRs are recruited into and retained within postsynaptic AChR aggregates.

Changes in the amount of postsynaptic rapsyn may modulate the rate of metabolic turnover of associated AChRs. Ongoing synaptic transmission serves to maintain the slow metabolic turnover characteristic of AChRs at the adult synapse (half-life ~10 days; (Rotzler et al., 1991). Neural agrin can also slow AChR turnover (Bezakova et al., 2001a). Might activity and neural agrin act via a common final effector to slow AChR turnover? One possibility is that AChRs are stabilized by an increase in the amount of postsynaptic rapsyn. In cultured cells, co-transfection of rapsyn with AChR caused a modest but significant slowing of AChR turnover (Phillips et al., 1997; Wang et al., 1999). When expression plasmid for rapsyn-EGFP was introduced into the tibialis anterior muscle of 1-month old mice the turnover of the postsynaptic AChRs was slowed (Gervásio and Phillips, 2005). As shown here, the slowing of AChR turnover depended upon the amount of rapsyn-EGFP in

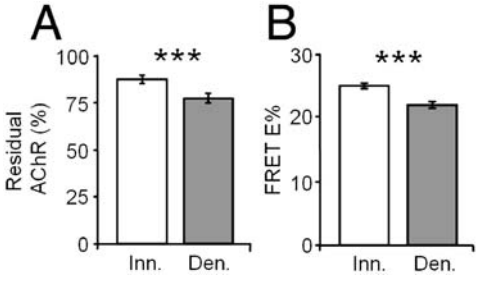

Fig. 9. Denervation reduced the fraction of postsynaptic AChRs that were resistant to detergent extraction. Tibialis anterior muscles were denervated by sciatic nerve resection at 1-month postnatal. Ten days later, transverse cryosections were fixed for 20 min in PBS containing 1 mg/ml saponin followed by further extraction with 1% Triton X100 (10 min at RT). Sections were then labeled with Alexa647-α-BGT. The intensity of postsynaptic AChR staining was normalized to that of sections fixed in the absence of detergent. (A) The intensity of Alexa647-α-BGT fluorescence of extracted endplates was expressed as a fraction of the fluorescence of endplates on non-extracted sister sections to derive the percentage of resistant AChRs. (B) FRET efficiency (FRET E%) data reproduced from Fig. 8E for comparison. Error bars in panel A represent the mean ± SEM for 4 mice with minimum of 10 synapses per mouse (***$P<0.001$; Student's *t*-test).

the postsynaptic membrane: those synapses with the most rapsyn-EGFP retained more of their α-BGT-labeled AChR for longer (Figs. 1D, E). During normal postnatal development the rapsyn-to-AChR immunofluorescence ratio rose about two-fold, leveling off at about 1-month postnatal (Fig. 2B). Denervation of 1-month postnatal muscles led to a reduction in the postsynaptic rapsyn-to-AChR immunofluorescence ratio. Reductions were evident using antibodies that recognize two distinct epitopes on rapsyn (Fig. 5E), strongly suggesting that there were fewer molecules of rapsyn per AChR in the denervated postsynaptic membrane. Furthermore, after muscles were electroporated with expression plasmid, the amount of rapsyn-EGFP fluorescence that accumulated at denervated endplates was 53% lower than for innervated contralateral endplates (see Results). Again this suggests that ongoing innervation is needed for optimal targeting of rapsyn to the postsynaptic membrane. Differences in rapsyn-to-AChR ratio of a similar magnitude (i.e. about two-fold) were sufficient to slow AChR turnover in (innervated) muscle fibers expressing rapsyn-EGFP (Fig. 1D; (Gervásio and Phillips, 2005). Thus, the normal developmental changes in the postsynaptic rapsyn-to-AChR ratio are likely to be functionally significant. The absolute stoichiometry (how many molecules of rapsyn are bound to each postsynaptic AChR) remains to be determined.

FRET analysis provides a measure of the efficiency of AChR aggregation. The AChR-rich area of the synapse is composed of discontinuous AChR aggregates separated by postjunctional membrane infoldings that could not be easily resolved without electron microscopy (Salpeter and Harris, 1983). Even electron microscopic labeling techniques do not normally resolve individual AChR aggregates, but rather AChR-rich membrane domains. For this reason the intensity of fluorescent-α-BGT labeling does not necessarily reflect the degree of (sub-microscopic) AChR aggregation. In contrast, energy transfer in FRET occurs only when the donor and acceptor fluorophors are separated by less than 100 Å (Sekar and Periasamy, 2003). We have developed a confocal-based FRET method for assessing the degree to which AChRs are clustered. This involves by randomly labeling the two binding sites on each AChR with fluorescently conjugated α-BGT. Several lines of evidence suggest that the developmental increase in FRET efficiencies reflects enhanced postsynaptic AChR aggregation: (1) no FRET occurred if the donor/acceptor toxin mix was allowed to bind to a glass surface in the absence of AChRs, (2) while the relationship between FRET efficiency and donor–acceptor distance is problematic (as discussed below) the FRET efficiencies at mature synapses using either FRET pair were too high to be easily explained by intra-receptor FRET, (3) FRET revealed a highly significant developmental increase in postsynaptic FRET efficiency that was partially reversible by denervation, (4) in situations where AChRs were enriched but not immobilized in aggregates (intracellular AChRs beneath the postsynaptic membrane, perisynaptic AChRs and AChRs expressed in QT-6 fibroblasts), FRET efficiencies were significantly lower than in the adult postsynaptic membrane (Figs. 8D, E).

The confocal FRET assay reveals changes in the organization of postsynaptic AChR aggregates but is not suited to measuring the absolute spacing between adjacent AChRs. The theoretical relationship between FRET efficiency and the distance between donor and acceptor fluorophor depends upon the Förster distance for a particular FRET pair (R_o, Materials and methods). Unfortunately, estimates of R_o depend upon (among other things) the experimentally determined: quantum efficiency of the donor, absorption spectrum of the acceptor and the orientation factor for the fluorophor pair *in situ*. These three factors in particular can be influenced by the molecular environment (Panchuk-Voloshina et al., 1999; Soper et al., 1993) but are difficult to measure *in situ*, using confocal microscopy. They may differ substantially from published values when the fluorophors are attached to a specific protein and embedded in a cellular structure. Depending upon which published values for such parameters were used, estimates of the donor–acceptor distance ranged from 61 Å to 76 Å. However, the FRET efficiencies we record will also systematically underestimate the real potential for energy transfer between adjacent toxin-AChRs complexes. AChRs are randomly labeled with a mixture of donor- and acceptor-conjugated α-bungarotoxin applied in a molar ratio of 1:4 to maximize FRET efficiency (see Materials and methods). This means that four out of five times a donor fluorophor will bind to an AChR and be adjacent to an acceptor as shown in Fig. 8A. However, one in five donors will, by chance have a donor as its nearest neighbor (rather than an acceptor) and be unable to engage in efficient FRET. Finally, within the AChR aggregate, the toxin-binding alpha-subunits of adjacent AChRs are likely to be rotationally offset from each other (cf. Fig. 8A), reducing the efficiency of inter-AChR FRET by an uncertain amount. Despite these caveats, the significant changes in synaptic FRET efficiency, during development and after denervation, provide evidence of some form of reorganization of the postsynaptic AChR aggregates as the synapse matures.

Changes in FRET efficiency may reflect either altered AChR-AChR spacing or recruitment and retention of AChRs by post-

synaptic AChR aggregates. In calculating FRET, energy transfer must be normalized to the AChR level (unquenched donor fluorophor intensity; Eq. (a), Materials and methods). For this reason the calculated FRET efficiency depends linearly upon what fraction of the AChRs are aggregated. Non-aggregated AChRs count toward AChR level but contribute little to FRET. Thus the developmental increase in FRET efficiency may be due either to closer packing of adjacent AChRs within AChR aggregates, or to incorporation of a greater fraction of the mobile (non-aggregated) postsynaptic AChR population into AChR aggregates, or both. The measured developmental increase in FRET (Fig. 2C) could conceivably be caused by a reduction in average donor–acceptor spacing. On the other hand, electron microscopic autoradiography counts detected no change in the density of AChRs (about 9000 per μm^2 of postjunctional thickenings) in the extensor digitorum longus muscle during postnatal development (Mathews-Bellinger and Salpeter, 1983). Alternatively, the developmental increase in FRET efficiency in the first month postnatal (Figs. 2C and 8E) might be explained by more efficient sequestration of inserted mobile postsynaptic AChRs into the maturing AChR aggregates. The drop in FRET efficiency following denervation (Fig. 8D) probably reflected a regression to less efficient sequestration of AChRs within AChR aggregates, since it was matched by a commensurate reduction in the fraction of postsynaptic AChRs that were resistant to detergent extraction (Fig. 9, compare A and B). Extra AChRs were added to the postsynaptic membrane following denervation (Figs. 4B, C), but there was less rapsyn for each postsynaptic AChR (Fig. 5). One possibility requiring further investigation is that a high ratio of rapsyn-to-AChR is necessary for efficient sequestration of postsynaptic AChRs into AChR aggregates.

FRET may reveal quantitative changes in postsynaptic receptor aggregation in health and disease. Mutations to the genes for either MuSK or rapsyn can lead to congenital Myasthenia Gravis, with gross impairment of the postsynaptic AChR-rich area (Chevessier et al., 2004; Ohno et al., 2002). FRET may allow us to detect more subtle abnormalities in postsynaptic receptor aggregation. For example, patient auto-antibodies against MuSK are proposed to cause autoimmune Myasthenia Gravis (Hoch et al., 2001) but the postsynaptic AChR clusters of such patients appeared largely normal (Selcen et al., 2004; Shiraishi et al., 2005). It may be valuable to develop analogous FRET assays to study other kinds of receptors. Submicroscopic changes in the degree of postsynaptic receptor aggregation could conceivably constitute another form of synaptic plasticity in the brain.

How might developmental changes in the amount of postsynaptic rapsyn influence AChR aggregation? The efficiency of FRET rose in parallel with the rapsyn-to-AChR immunofluorescence ratio during development, and both measures declined after denervation, consistent with the possibility that changes in the latter may have caused the former. The targeting of extra molecules of rapsyn to each postsynaptic AChR could be expected to enhance rapsyn-mediated linkage to other proteins. The tetratrico peptide repeats (TPRs) that mediate rapsyn self-association might have forged extra cross-links between adjacent rapsyn–AChR complexes (Eckler et al., 2005; Ramarao et al., 2001). The additional rapsyn RING-H2 domains might have tethered AChR–rapsyn complexes more effectively (via β-dystroglycan) to α-dystrobrevin and other proteins that are known to be necessary for AChR stability (Akaaboune et al., 2002; Bartoli et al., 2001). It will be important to experimentally test these ideas by perturbing the level of rapsyn expression during the first month of postnatal life. Postnatal synaptic development also involves growth of secondary postjunctional membrane folds, and these folds were reduced in patients with point mutations to rapsyn (Ohno et al., 2002; Yasaki et al., 2003). Thus, it is conceivable that changes in AChR aggregation (detected by FRET) and in AChR turnover may involve altered postjunctional folding.

Fig. 10 outlines a hypothetical model for how AChRs may be managed within the postsynaptic membrane. The postsynaptic membrane is divided into alternating membrane domains: AChR-aggregate-containing domains, and membrane infoldings. The latter contain a pool of mobile AChRs. There appears to be a slow interchange of AChRs between these domains (Fig. 10, see two-way arrows; Akaaboune et al., 1999, 2002). The developmental increase in FRET efficiency may reflect a greater proportion of postsynaptic AChRs being incorporated into aggregates as the synapse matures. Increased targeting of rapsyn to

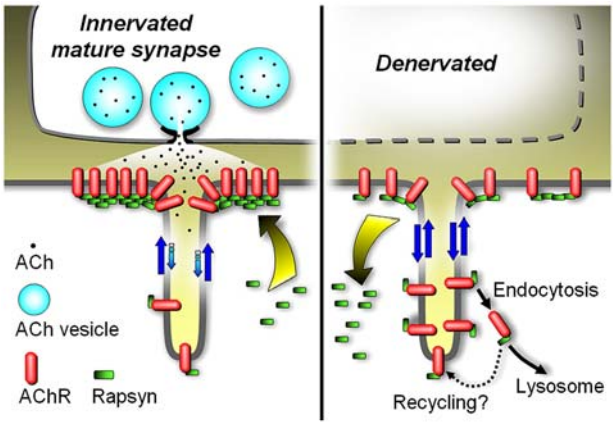

Fig. 10. A hypothetical model for how AChRs may be managed in the postsynaptic membrane (see Discussion). The AChR-rich postsynaptic membrane consists of domains containing immobile aggregates of rapsyn and AChR. AChRs within these aggregate domains are in constant, albeit slow, interchange with a pool of surface-exposed but non-aggregated AChRs scattered through membrane infoldings and in the perisynaptic membrane (two-way arrows; Akaaboune et al., 2002). Some rapsyn binds the AChR during AChR biosynthesis (Marchand et al., 2002) forming a basal rapsyn–AChR complex (perhaps ~1:1 stoichiometry) but the amount of rapsyn bound to each AChR may increase in response to neural agrin (Moransard et al., 2003; Zhu et al., 2006). Our results suggest that during postnatal synaptic maturation, the ratio of rapsyn-to-AChR within the postsynaptic membrane increases still further, enhancing the recruitment and retention of AChRs in AChR aggregates, and ensuring slow AChR turnover (left hand panel). Denervation reverses this process (right panel). A reduction in postsynaptic rapsyn (curved arrow) may cause accelerated loss of AChR (turnover) by making postsynaptic AChR more available for endocytic capture. Alternatively, since synaptic AChR may be constantly recycling (Bruneau et al., 2005), less rapsyn bound to each AChR might bias the routing of internalized AChRs, to favor more lysosomal degradation. Thus the developmental increase in the rapsyn-to-AChR ratio may help drive the transition of immature AChR plaques into the tightly packed, stable AChR aggregate structures characteristic of the mature synapse.

the postsynaptic membrane may drive this enhanced AChR aggregation (curved arrow in left panel). The decline in postsynaptic rapsyn after denervation (Fig. 10, right panel) might help to explain the associated reduction in FRET efficiency. Artificially increasing the amount of postsynaptic rapsyn slowed AChR turnover (Fig. 1; Gervásio and Phillips, 2005). Conversely, the reduction in postsynaptic rapsyn that occurred after denervation (Fig. 5) may have caused the accelerated AChR turnover. The faster loss of synaptic AChR may be secondary to the less efficient sequestration of AChRs into aggregates, since this would make a greater fraction of postsynaptic AChRs vulnerable to internalization (Fig. 10, right panel). Alternatively, since postsynaptic AChRs undergo recycling through an endosome compartment (Bruneau et al., 2005), a reduction in the amount of rapsyn bound to each AChR might influence the intracellular trafficking of internalized AChR–rapsyn complex, favoring the lysosome path (Fig. 10, right hand side).

In a rat model of autoimmune Myasthenia Gravis, electroporation of muscles with rapsyn protected synapses from anti-AChR autoantibody attack (Losen et al., 2005). Thus, the molecular mechanisms that control postsynaptic rapsyn-to-AChR ratio also have relevance to developing treatments for synaptic dysfunction. Cell culture studies suggest that neural agrin signaling can increase the amount of rapsyn targeted to AChRs on the plasma membrane, and that Src family kinases may be involved (Moransard et al., 2003; Sadasivam et al., 2005). We now need a more detailed understanding of the mechanisms that control targeting of rapsyn to the postsynaptic membrane, and thus AChR aggregation.

Acknowledgments

The authors would like to thank Ellie Kable of the University of Sydney Electron Microscope Unit for help with confocal microscopy, Peter Noakes for critical reading of the manuscript and Cristobal Dos Remedios and Samuel Solomon for their help with FRET calculations. This work was supported by a grant from the NH&MRC (Australia) to WDP.

References

Akaaboune, M., Culican, S.M., Turney, S.G., Lichtman, J.W., 1999. Rapid and reversible effects of activity on acetylcholine receptor density at the neuromuscular junction in vivo. Science 286, 503–507.

Akaaboune, M., Grady, R.M., Turney, S., Sanes, J.R., Lichtman, J.W., 2002. Neurotransmitter receptor dynamics studied in vivo by reversible photounbinding of fluorescent ligands. Neuron 34, 865–876.

Bartoli, M., Ramarao, M.K., Cohen, J.B., 2001. Interactions of the rapsyn RING-H2 domain with dystroglycan. J. Biol. Chem. 276, 24911–24917.

Bastiaens, P.I., Majoul, I.V., Verveer, P.J., Soling, H.D., Jovin, T.M., 1996. Imaging the intracellular trafficking and state of the AB5 quaternary structure of cholera toxin. EMBO J. 15, 4246–4253.

Berg, D.K., Hall, Z.W., 1975. Loss of alpha-bungarotoxin from junctional and extrajunctional acetylcholine receptors in rat diaphragm muscle in vivo and in organ culture. J. Physiol. 252, 771–789.

Bezakova, G., Ruegg, M.A., 2003. New insights into the roles of agrin. Nat. Rev., Cell Mol. Biol. 4, 295–308.

Bezakova, G., Helm, J.P., Francolini, M., Lomo, T., 2001a. Effects of purified recombinant neural and muscle agrin on skeletal muscle fibers in vivo. J. Cell Biol. 153, 1441–1452.

Bezakova, G., Rabben, I., Sefland, I., Fumagalli, G., Lomo, T., 2001b. Neural agrin controls acetylcholine receptor stability in skeletal muscle fibers. Proc. Natl. Acad. Sci. U. S. A. 98, 9924–9929.

Bruneau, E., Sutter, D., Hume, R.I., Akaaboune, M., 2005. Identification of nicotinic acetylcholine receptor recycling and its role in maintaining receptor density at the neuromuscular junction in vivo. J. Neurosci. 25, 9949–9959.

Burden, S.J., DePalma, R.L., Gottesman, G.S., 1983. Crosslinking of proteins in acetylcholine receptor-rich membrane: association between the β-subunit and the 43 kd subsynaptic protein. Cell 35, 687–692.

Campagna, J.A., Fallon, J., 2006. Lipid rafts are involved in C95 (4,8) agrin fragment-induced acetylcholine receptor clustering. Neuroscience 138, 123–132.

Chevessier, F., Faraut, B., Ravel-Chapuis, A., Richard, P., Gaudon, K., Bauche, S., Prioleau, C., Herbst, R., Goillot, E., Ioos, C., Azulay, J.P., Attarian, S., Leroy, J.P., Fournier, E., Legay, C., Schaeffer, L., Koenig, J., Fardeau, M., Eymard, B., Pouget, J., Hantai, D., 2004. MUSK, a new target for mutations causing congenital myasthenic syndrome. Hum. Mol. Genet. 13, 3229–3240.

Eckler, S.A., Kuehn, R., Gautam, M., 2005. Deletion of N-terminal rapsyn domains disrupts clustering and has dominant negative effects on clustering of full-length rapsyn. Neuroscience 131, 661–670.

Froehner, S.C., Luetje, C.W., Scotland, P.B., Patrick, J., 1990. The postsynaptic 43K protein clusters muscle nicotinic acetylcholine receptors in *Xenopus* oocytes. Neuron 5, 403–410.

Gautam, M., Noakes, P.G., Mudd, J., Nichol, M., Chu, G.C., Sanes, J.R., Merlie, J.P., 1995. Failure of postsynaptic specialization to develop at neuromuscular junctions of rapsyn deficient mice. Nature 377, 232–236.

Gautam, M., Noakes, P.G., Moscoso, L., Rupp, F., Scheller, R.H., Merlie, J.P., Sanes, J.R., 1996. Defective neuromuscular synaptogenesis in agrin-deficient mutant mice. Cell 85, 525–535.

Gervásio, O.L., Phillips, W.D., 2005. Increased ratio of rapsyn to ACh receptor stabilizes postsynaptic receptors at the mouse neuromuscular synapse. J. Physiol. 562.3, 673–685.

Glass, D.J., Bowen, D.C., Stitt, T.N., Radiejewski, C., Brunno, J., Ryan, T.E., Gies, D.R., Shah, S., Mattsson, K., Burden, S.J., DiStefano, P.S., Valenzuela, D.M., DeChiara, T.M., Yancopoulos, G.D., 1996. Agrin acts via a MuSK receptor complex. Cell 85, 513–523.

Hoch, W., McConville, J., Helms, S., Newsom-Davis, J., Melms, A., Vincent, A., 2001. Autoantibodies to the receptor tyrosine kinase MuSK in patients with myasthenia gravis without acetylcholine receptor antibodies. Nat. Med. 7, 365–368.

Kenworthy, A.K., 2001. Imaging protein-protein interactions using fluorescence resonance energy transfer microscopy. Methods 24, 289–296.

Land, B.R., Salpeter, E.E., Salpeter, M.M., 1980. Acetylcholine receptor site density affects the rising phase of miniature endplate currents. Proc. Natl. Acad. Sci. U. S. A. 77, 3736–3740.

LaRochelle, W.J., Froehner, S.C., 1987. Comparison of the postsynaptic 43-kDa protein from muscle cells that differ in acetylcholine receptor clustering activity. J. Biol. Chem. 262, 8190–8195.

Lin, W., Dominguez, B., Yang, J., Aryal, P., Brandon, E.P., Gage, F.H., Leem, K.-F., 2005. Neurotransmitter acetylcholine negatively regulates neuromuscular synapse formation by a Cdk5-dependent mechanism. Neuron 46, 569–579.

Losen, M., Stassen, M.H.W., Martinez-Martinez, P., Machiels, B., Duimel, H., Frederik, P., Veldman, H., Wokke, J.H.J., Spaans, F., Vincent, A., DeBaets, M., 2005. Increased expression of rapsyn in muscles prevents acetylcholine receptor loss in experimental autoimmune myasthenia gravis. Brain 128, 2327–2337.

Marchand, S., Devillers-Thiery, A., Pons, S., Changeux, J.-P., Cartaud, J., 2002. Rapsyn escorts the nicotinic acetylcholine receptor along the exocytic pathway via association with lipid rafts. J. Cell Biol. 22, 8891–8901.

Mathews-Bellinger, J.A., Salpeter, M.M., 1983. Fine structural distribution of acetylcholine receptors at developing mouse neuromuscular junctions. J. Neurosci. 3, 644–657.

Mitra, A.K., McCarthy, M.P., Stroud, R.M., 1989. Three-dimensional structure of the nicotinic acetylcholine receptor and location of the major associated 43-kD cytoskeletal protein, determined at 22Å by low dose electron microscopy and X-ray diffraction to 12.5A. J. Cell Biol. 109, 755–774.

Moransard, M., Borges, L.S., Willmann, R., Marangi, P.A., Brenner, H.R.,

Ferns, M.J., Fuhrer, C., 2003. Agrin regulates rapsyn interaction with surface AChRs which underlies cytoskeletal anchoring and clustering. J. Biol. Chem. 278, 7350–7359.

Noakes, P.G., Chin, D., Kim, S.S., Liang, S., Phillips, W.D., 1999. Expression and localisation of dynamin and syntaxin during neural development and neuromuscular synapse formation. J. Comp. Neurol. 410, 531–540.

Ohno, K., Engel, A.G., Shen, X.-M., Selcen, D., Brengman, J., Harper, C.M., Tsujino, A., Milone, M., 2002. Rapsyn mutations in humans cause endplate acetylcholine-receptor deficiency and myasthenic syndrome. Am. J. Hum. Genet. 70, 875–885.

Paas, Y., Cartaud, J., Recouvreur, M., Grailhe, R., Dufresne, V., Pebay-Peyroula, E., Landau, E.M., Changeux, J.P., 2003. Electron microscopic evidence for nucleation and growth of 3D acetylcholine receptor microcrystals in structured lipid-detergent matrices. Proc. Natl. Acad. Sci. U. S. A. 100, 11309–11314.

Panchuk-Voloshina, N., Haugland, R.P., Bishop-Stewart, J., Bhalgat, M.K., Millard, P.J., Mao, F., Leung, W.-Y., Haugland, R.P., 1999. Alexa dyes, a series of new fluorescent dyes that yield exceptionally bright, photostable conjugates. J. Histochem. Cytochem. 47, 1179–1188.

Phillips, W.D., Kopta, C., Blount, P., Gardner, P.D., Steinbach, J.H., Merlie, J.P., 1991. ACh receptor-rich membrane domains organized in fibroblasts by recombinant 43-kilodalton protein. Science 251, 568–570.

Phillips, W.D., Noakes, P.G., Roberds, S.L., Campbell, K.P., Merlie, J.P., 1993. Clustering and immobilization of acetylcholine receptors by the 43-kD protein: a role for dystrophin-related protein. J. Cell Biol. 123, 729–740.

Phillips, W.D., Vladeta, D., Han, H., Noakes, P.G., 1997. Rapsyn and agrin slow the metabolic degradation of the acetylcholine receptor. Mol. Cell. Neurosci. 10, 16–26.

Ramarao, M.K., Bianchetta, M.J., Lanken, J., Cohen, J.B., 2001. Role of rapsyn tetratrico repeat and coiled-coil domains in self association and nicotinic acetylcholine receptor clustering. J. Biol. Chem. 276, 7475–7483.

Rotzler, S., Schramek, H., Brenner, H.R., 1991. Metabolic stabilization of endplate acetylcholine receptors regulated by Ca2+ influx associated with muscle activity. Nature 349, 337–339.

Sadasivam, G., Willman, R., Lin, S., Erb-Vogtli, S., Kong, X.C., Ruegg, M.A., Fuhrer, C., 2005. Src-family kinases stabilize the neuromuscular synapse via protein interactions, phosphorylation, and cytoskeletal linkage. J. Neurosci. 25, 10479–10493.

Salpeter, M.M., Harris, R., 1983. Distribution and turnover rate of acetylcholine receptors throughout the junction folds at a vertebrate neuromuscular junction. J. Cell Biol. 96, 1781–1785.

Samson, A.O., Scherf, T., Eisenstein, M., Chill, J.H., Anglister, J., 2002. The mechanism for acetylhcoline receptor inhibition by α-neurotoxins and species-specific resistance to α-bungarotoxin revealed by NMR. Neuron 35, 319–332.

Sanes, J.R., Lichtman, J.W., 2001. Induction, assembly, maturation and maintenance of a postsynaptic apparatus. Nat. Rev., Neurosci. 2, 791–805.

Sekar, R.B., Periasamy, A., 2003. Fluorescence resonance energy transfer (FRET) microscopy imaging of live cell protein localizations. J. Cell Biol. 160, 629–633.

Selcen, D., Fukuda, T., Shen, X.-M., Engel, A.G., 2004. Are MuSK antibodies the primary cause of myasthenic symptoms? Neurology 62, 1945–1950.

Shiraishi, H., Motomura, M., Yoshimura, T., Fukudome, T., Fukuda, T., Nakao, Y., Tsujihata, M., Vincent, A., Eguchi, K., 2005. Acetylcholine receptors loss and postsynaptic damage in MuSK antibody-positive myasthenia gravis. Ann. Neurol. 57, 289–293.

Soper, S.A., Nutter, H.L., Keller, R.A., Davis, L.M., Shera, E.B., 1993. The photophysical constants of several fluorescent dyes pertaining to ultrasensitive fluorescence spectroscopy. Photochem. Photobiol. 57, 972–977.

Steigmiller, S., Zimmermann, B., Diez, M., Borsch, M., Graber, P., 2004. Binding of single nucleotides to H+-ATP synthases observed by fluorescence resonance energy transfer. Bioelectrochemistry 63, 79–85.

Strochlic, L., Cartaud, A., Cartaud, J., 2005. The synaptic muscle-specific kinase (MuSK) complex: new partners, new functions. BioEssays 27, 1129–1135.

Szabo, M., Salpeter, E.E., Randall, W., Salpeter, M.M., 2003. Transients in acetylcholine receptor site density and degradation during reinnervation of mouse sternomastoid muscle. J. Neurochem. 84, 180–188.

Van Der Meer, B.W., Coker III, G., Chen, S.-Y.S., 1994. Resonance Energy Transfer Theory and Data. VCH Publishers, Inc., New York.

Wallrabe, H., Elangovan, M., Burchard, A., Periasamy, A., Barroso, M., 2003a. Confocal FRET microscopy to measure clustering of ligand–receptor complexes in endocytic membranes. Biophys. J. 85, 559–571.

Wallrabe, H., Stanley, M., Periasamy, A., Barroso, M., 2003b. One- and two-photon fluorescence resonance energy transfer microscopy to establish a clustered distribution of receptor–ligand complexes in endocytic membranes. J. Biomed. Opt. 8, 339–346.

Wang, Z.Z., Mathias, A., Gautam, M., Hall, Z.W., 1999. Metabolic stabilization of muscle nicotinic acetylcholine receptor by rapsyn. J. Neurosci. 19, 1998–2007.

Yasaki, E., Prioleau, C., Barbier, J., Richard, P., Andreux, F., Leroy, J.-P., Dartevelle, P., Koenig, J., Molgo, J., Fardeau, M., Eymard, B., Hantai, D., 2003. Electrophysiological and morphological characterization of a case of autosomal recessive congenital myasthenic syndrome with acetylcholine receptor deficiency due to N88K rapsyn homozygous mutation. Neuromuscul. Disord. 14, 24–32.

Zhu, D., Xiong, W.C., Mei, L., 2006. Lipid rafts serve as a signaling platform for nicotinic acetylcholine receptor clustering. J. Neurosci. 26, 4841–4851.